Available online at www.sciencedirect.com
SCIENCE DIRECT®
Journal of the European Ceramic Society 25 (2005) 2191–2196
www.elsevier.com/locate/jeurceramsoc

Correlation between oxygen transport properties and microstructure in $La_{0.5}Sr_{0.5}FeO_{3-\delta}$

Stefan Diethelm [a,*], Jan Van herle [a], Joseph Sfeir [b,1], Philippe Buffat [c]

[a] *Laboratory for Industrial Energy Systems (LENI), STI, Swiss Federal Institute of Technology, CH-1015 Lausanne, Switzerland*
[b] *HTceramix, EPFL Science Park, PSE-A, CH-1015 Lausanne, Switzerland*
[c] *Interdisciplinary Centre for Electron Microscopy (CIME), SB, Swiss Federal Institute of Technology, CH-1015 Lausanne, Switzerland*

Available online 23 March 2005

Abstract

The effect of the bulk microstructure (grain size distribution, grain boundary composition) on the oxygen transport properties of $La_{0.5}Sr_{0.5}FeO_3$ membranes was investigated. For this purpose, samples with different microstructures were prepared by modifying the sintering duration and/or temperature. The average grain sizes, ranging from 0.20 to 1.43 μm, were determined from SEM analysis. The oxygen transport properties of these samples were characterised by permeation measurement. The fluxes presented a change in the activation energy which was attributed to a change in the rate limiting step, from bulk diffusion at lower temperature (<850 °C) to surface limitations at higher temperature (>900 °C). Only the transport through the bulk was influenced by the microstructure, with the highest flux for the smallest grains. This would imply that oxygen transport occurs more rapidly along the grain boundaries than through the bulk. Grain and grain boundary compositions were analysed by TEM.

Keywords: Grain growth; Grain size; Grain boundaries; Ionic conductivity; Perovskites

1. Introduction

Perovskite-type mixed conducting oxides have been intensively studied in view of their application as oxygen separation membranes[1] or cathodes in solid oxide fuel cells.[2] In particular, the oxygen transport properties of a large variety of compositions have been investigated. However, a review of this abundant literature data often reveals important discrepancies, especially for identical compositions.[3] These discrepancies are believed to arise from differences in the microstructure of the samples. The influence of the microstructure on the oxygen transport properties of mixed conducting oxides has often been ignored, but recently, several studies have pointed out its importance. The microstructure, i.e. grain size distribution, inhomogeneous grain composition or grain boundary composition, depends significantly on the preparation method and the sintering procedure. As an example, Zhang et al.[4,5] have obtained samples of $SrFe_{0.2}Co_{0.8}O_{3-\delta}$ with grain sizes comprised between 2 and 15 μm by varying sintering temperature between 930 and 1200 °C. Permeation measurements showed that the oxygen flux could be increased by a factor 3 simply by decreasing the grain size. They suggested that the grain boundaries provided high diffusivity paths due to higher defect concentrations. The opposite trend was observed by Kharton et al.[6] in $La_{0.3}Sr_{0.7}CoO_{3-\delta}$. For instance, the permeability through a 80 μm grained sample was five times higher than through a 20 μm grained sample. This pointed to grain boundary resistance to oxygen ion transport. Nevertheless, fast diffusion along the grain boundary was also reported for a 3–4 μm grained sample, which had undergone liquid phase sintering, giving grain boundaries of distinctly different composition than that of the bulk. The influence of the powder synthesis method on the microstructure was further investigated by Qi et al.[7] Although different microstructures were thus obtained (with average grain size varying from 1 to 5 μm), little flux variation was noticed. Therefore, grain boundaries can either

* Corresponding author. Tel.: +41 216935968; fax: +41 216933502.
E-mail address: stefan.diethelm@epfl.ch (S. Diethelm).
[1] Present address: Laboratory For High Performance Ceramics, EMPA, Dübendorf, Ueberlandstrasse 129, CH-8600 Dübendorf, Switzerland.

0955-2219/$ – see front matter © 2005 Elsevier Ltd. All rights reserved.
doi:10.1016/j.jeurceramsoc.2005.03.028

act as high diffusivity paths or barriers for oxygen transport depending on their structure and composition.

In this study, we examine the effect of microstructure on the oxygen transport properties of $La_{0.5}Sr_{0.5}FeO_{3-\delta}$ samples. In particular, the influence of the grain size and the grain boundary length (GBL) on the oxygen permeation flux is investigated.

2. Experimental

2.1. Sample preparation

The nanometric $La_{0.5}Sr_{0.5}FeO_{3-\delta}$ powder (~100 nm average grain size) was provided by HTceramix SA (Switzerland). Disc-shaped samples (30 mm diameter) were produced by uni-axial compaction of the powder at 50 MPa and sintered in air. The temperature and duration of the sintering were varied between 1175 and 1300 °C, respectively, 0.5 and 68 h, in order to control the microstructure. The density of the sintered samples was measured by the Archimedes method.

2.2. Permeation measurements

The oxygen transport through the dense samples was characterised by permeation measurements. A ~24 mm diameter dense sample was clamped between two alumina tubes using gold rings and paste as sealing.[8] Air was flushed in the lower compartment and argon in the upper one. Oxygen was separated from air by solid-state diffusion through the membrane and released in the argon side due to the oxygen partial pressure gradient. The extremities of the tubes were sealed in the cold. The outlet gas composition was analysed with a gas chromatograph from Varian Inc. equipped with a molecular sieve 5 Å capillary column. The outlet flux was measured online by a bubble-meter. Any leakage could be detected by the presence of N_2 in the outlet gas.

2.3. TEM observations

The sample was first mechanically polished down to approximately 20 μm using the tripod method. It was then thinned by ion milling under grazing incidence with full sample rotation in a Fischione apparatus at low temperature (close to liquefied nitrogen). The process started with a 5 mA beam of 6 keV Ar^+ ions. To reduce the milling artefacts, the ion energy was reduced to 3.0 keV for 30 min followed by 20 min at 0.5 keV at the end of the thinning process.

All TEM observations were done on a Philips CM300 FEG/UT microscope, with a field emission gun operated at 300 kV and a reduced illumination intensity (spot size 5 and above). The EDS standardless microanalysis was performed with an INCA/Oxford spectrometer.

3. Results and discussion

3.1. Grain growth

The microstructure of the samples, principally the grain size, was controlled by varying the sintering parameters, i.e. temperature and duration. The grain size distributions were estimated from SEM micrographs of the surface of the samples, using the following approach: the 2D surface area and periphery of the individual grains were first calculated with a graphical integrator software (DigitalMicrograph 3.4). Then, for the sake of simplicity, the grains were assimilated to cubes so that their characteristic dimension was taken as the side of a surface-equivalent-square. The grain boundary length was estimated from half of the perimeter of the grains per surface area and is thus expressed in $\mu m/\mu m^2$. It is evident that estimating the size of 3D grains from their planar section leads to an underestimation. It is, sometimes, possible to recover the real 3D grain-size distribution whenever the shape of the grain is known.[9] In this work, however, we shall remain with the 2D approximation. The resulting data is summarized in Table 1, for five different samples. In the remaining of this paper, the samples will be referred to by the following code: LSF-1200-1/2 corresponds to the $La_{0.5}Sr_{0.5}FeO_{3-\delta}$ sample, sintered at 1200 °C for half an hour, LSF-1250-15 corresponds to the $La_{0.5}Sr_{0.5}FeO_{3-\delta}$ sample, sintered at 1250 °C for 15 h, etc.

As the grain growth results from the free-energy difference across a curved grain boundary, its rate is expected to be inversely proportional to grain size and thermally activated in such a way that the grain size (d) can be expressed as[10]

$$d - d_0 = \sqrt{2r_0}\,\exp\left(-\frac{E_A}{RT}\right)\sqrt{t} \quad (1)$$

where d_0 is the initial grain size; r_0, pre-exponential factor of the rate of grain growth; E_A, activation energy; T, absolute temperature and t, sintering duration. In Fig. 1, the average grain size is plotted as a function of the sintering temper-

Table 1
Sintering parameters with the resulting grain size and grain boundary length

Sample	Sintering temperature (°C)	Sintering duration (h)	Average grain size[a] (μm)	GB length ($\mu m/\mu m^2$)
LSF-1200-1/2	1200	0.5	0.20 (0.10)	8.69
LSF-1200-2	1200	2	0.31 (0.15)	5.51
LSF-1200-20	1200	20	0.63 (0.26)	2.92
LSF-1250-15	1250	15	1.43 (0.64)	1.21
LSF-1275-15	1275	15	2.74 (1.15)	1.06

[a] Side of an area equivalent square. The standard deviation is given between parenthesis.

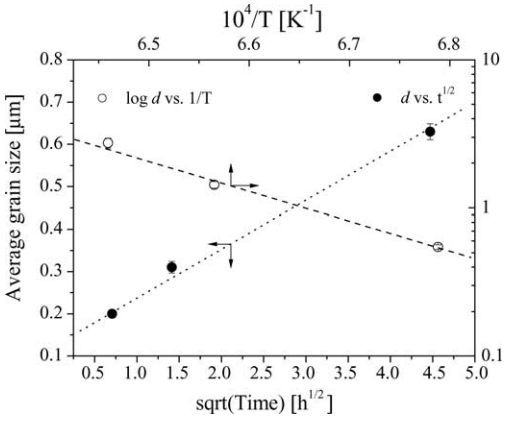

Fig. 1. Influence of the sintering temperature and duration on the average grain size, showing a $\sqrt{t}$ dependence and a thermal activation in accordance with Eq. (1).

ature and duration, showing that it effectively follows Eq. (1), with $d_0 = 0.121$ (7) µm, $k_0 = 3.9\ 10^9$ m^2/s and $E_A = 385$ (17) kJ/mol. The value of the initial grain size, d_0, is consistent with the average grain size of the starting powder.

In the sample that was sintered during 68 h at 1175 °C, as well as in those sintered at higher temperature (≥1250 °C), exsolution of a Fe-enriched phase (possibly iron oxide) was observed at the intersection of grains. This probably originates from a slight iron excess in the powder composition, as indicated by ICP. Finally, a sample that had been sintered for 10 h at 1300 °C had started to melt.

3.2. Oxygen permeation

The characteristics of the three membranes used for the permeation measurements are given in Table 2. The resulting oxygen fluxes are shown in an Arrhenius plot (Fig. 2) as a function of the inverse temperature. A change of the slope, which corresponds to a change in the activation energy (E_A), is clearly apparent around 900 °C for the LSF-1200-20 sample. This change was reproducible upon thermal cycling, which means that the permeation fluxes had reached their steady-state value.

In order to account for an eventual influence of the variation of the oxygen partial pressure p_{O_2} gradient due to the increase of the flux at high temperature, the overall oxygen transfer coefficients (K) were calculated using Wagner's equation for the permeation flux through mixed

Table 2
Characteristics of the membranes used for permeation measurements

Membrane	Pellet thickness (mm)	Density (g/cm^3)	Relative density (%)
LSF-1200-1/2	0.82 (2)	6.09	99.1
LSF-1200-20	0.94 (1)	6.09	99.1
LSF-1250-15	1.10 (2)	6.01	97.8

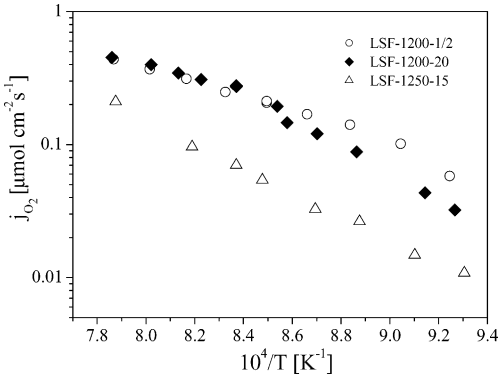

Fig. 2. Arrhenius plot of the oxygen permeation flux between 800 and 1000 °C through membranes with different microstructure.

conductors:[1,11]

$$j_{O_2} = -\frac{RT}{16F^2} K\, \Delta \ln p_{O_2} = -\frac{RT}{16F^2}\left[\frac{1}{\kappa'} + \frac{1}{\kappa''} + \frac{L}{\bar{\sigma}_{amb}}\right]^{-1} \Delta \ln p_{O_2} \quad (2)$$

where L is the membrane thickness; R, ideal gas constant and F, Faraday's constant. K is a combination of bulk and surface parameters and $\bar{\sigma}_{amb}$ is the mean value of the ambipolar conductivity coefficient, which describes the simultaneous transport of oxygen ions and electronic species in the membrane, and κ', respectively, and κ'', represent the surface exchange reaction rates at each surface. In predominantly electronic conductors, such as $La_{0.5}Sr_{0.5}FeO_{3-\delta}$,[12] $\sigma_{amb} \cong \sigma_i$, the ionic conductivity. As the local p_{O_2} difference is not directly measurable, it was replaced by a average logarithmic p_{O_2} difference in a similar way as a logarithmic temperature difference is defined in heat exchangers:[13]

$$\Delta \ln p_{O_2} = \ln \frac{p''_{O_2}}{p'_{O_2}} \cong \frac{\Delta \ln p_{O_2,in} - \Delta \ln p_{O_2,out}}{\ln(\Delta \ln p_{O_2,in}/\Delta \ln p_{O_2,out})} \quad (3)$$

where the subscript "in" refers to the fluxes entering the reactor, and "out" to those exiting it. The advantage of this expression is that it depends only on known or measurable quantities.

The resulting overall oxygen transfer coefficients, calculated from Eq. (2) are shown in Fig. 3. As the tested membranes had different thickness (cf. Table 2), the K values were also multiplied by the thickness to get normalised values. These are shown in Fig. 4. After this correction, the change in activation energy is still apparent.

A possible explanation of this change of slope would be that the material undergoes an order–disorder phase transformation around 900 °C. The transition between the high temperature perovskite-type phase, where the oxygen vacancies are randomly distributed, and the brownmillerite-type phase, where the oxygen vacancies are ordered,[1] is known to reduce dramatically the oxygen transport in such materials.[14] In order to check this assumption, TG-DTA measurements

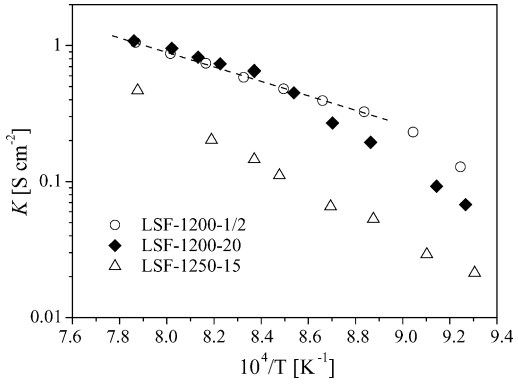

Fig. 3. Arrhenius plot of the global oxygen transport coefficient K for different samples. The line is a linear regression of the high temperature data of LSF-1200-1/2.

were carried out on the powder. As a sign of this transition, one would expect an endothermic peak around 900 °C during heating and an exothermic peak during cooling.[15] This, however, was not observed, neither in air nor in argon.

A similar change in activation energy was already observed with $La_{0.6}Ca_{0.4}Fe_{0.75}Co_{0.25}O_{3-\delta}$.[8] The comparison of the oxygen flux through membranes of different thickness revealed that the lower temperature data was inversely proportional to the thickness contrary to the higher temperature data. Thus, the former, which was characterised by higher activation energy, was attributed to bulk transport whereas the latter was attributed to surface limitation. For the present data, a similar explanation seems plausible. The coincidence of the K-values for LSF-1200-1/2 and LSF-1200-20 above 900 °C shows that they are independent of the samples' properties but rather representative of transport limitations occurring at the membrane/Ar interface. On the contrary, the lower temperature K-data depend strongly on the microstructure of the samples and are thus expected to be related to bulk transport. According to this interpretation, the LSF-1200-1/2 data would mainly be governed by surface limitation except at the lowest temperatures (≤825 °C). The LSF-1200-20 data would also be governed by surface limitation above 900 °C but by bulk transport below. Finally, the LSF-1250-15 data would be representative of bulk transport over the complete temperature range. The transition from the bulk-limited regime to the surface-limited regime when the temperature is increased results thus from the difference in their respective activation energies.

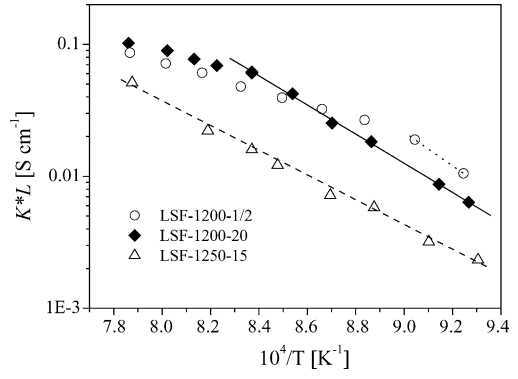

Fig. 4. Arrhenius plot of the normalised global oxygen transport coefficient (KL) corresponding to the contribution of bulk transport. The lines correspond to linear regressions of the data.

Table 3
Temperature dependence of the apparent ambipolar conductivity (σ_{amb}) and the surface rate constant (κ) obtained by linear regressions of the total transport coefficient (K) data

Grain size (μm)	$\sigma_{amb}T = a_{\sigma_0}\exp(-E_A/RT)$		$\kappa T = a_{\kappa_0}\exp(-E_A/RT)$	
	$\ln a_{\sigma_0}$ (S K/cm)	E_A (kJ/mol)	$\ln a_{\kappa_0}$ (S K/cm^2)	E_A (kJ/mol)
0.20	29 ± 2	243 ± 16	17.8 ± 0.2	112 ± 2
0.63	26.6 ± 0.4	221 ± 4	16.3 ± 0.4	96 ± 4
1.43	21.9 ± 0.6	188 ± 6	–	–

Based on the interpretation presented in the previous section, κ and σ_{amb} values were obtained by fitting the data plotted in Figs. 3 and 4 using Eq. (2), and are given in Table 3. The influence of the microstructure on the ambipolar conductivity is shown in Fig. 5 for two temperatures. The apparent conductivity decreases with increasing grain size and increases with increasing grain boundary length. This means that grain boundaries play a significant role in oxygen transport and offer a more rapid path. It is interesting to notice that the activation energy of the apparent conductivity increases as the grain size decreases, i.e. as the contribution of the grain boundaries becomes more important.

To allow further comparison with literature data, values of the diffusion coefficient for oxygen ions D_O were calculated using the Nernst–Einstein relation:

$$D_O = \frac{\sigma_i RT}{4C_O F^2} \quad (4)$$

These are given in Table 4. Thereby, it was assumed that $\sigma_{amb} \cong \sigma_i$, and use was made of the oxygen nonstoichiometry data from Mizusaki et al.[16] The most relevant literature data for us are tracer diffusion coefficients measured by Ishigaki et al.[17] for $La_{1-x}Sr_xFeO_{3-\delta}$ ($x = 0.1$, 0.25 and

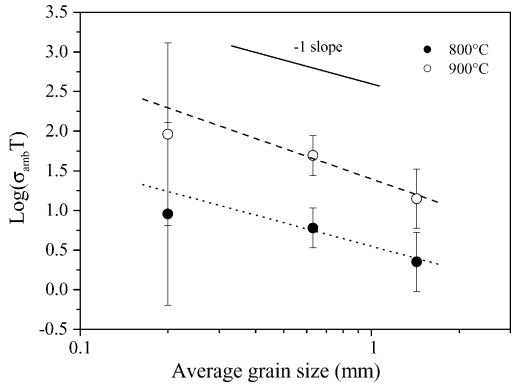

Fig. 5. Influence of the grain size on the apparent ambipolar conductivity (σ_{app}) at 800 and 900 °C. The lines correspond to a linear regression.

Table 4
Diffusion (D_O) and surface exchange (k_O) coefficients calculated from the σ_{amb} and κ data using Nerst–Einstein relation

T (°C)	D_O (cm^2/s)			k_O (cm/s)
	LSF-1200-1/2	LSF-1200-20	LSF-1250-15	
800	2.62×10^{-8}	1.74×10^{-8}	6.50×10^{-9}	(5.47×10^{-7})
900	(2.67×10^{-7})	1.44×10^{-7}	3.92×10^{-8}	1.60×10^{-6}
1000	(1.88×10^{-6})	(8.54×10^{-7})	1.78×10^{-7}	3.93×10^{-6}
E_A (kJ/mol)	243	221	188	112

The values between parenthesis are extrapolated.

0.4) single crystals. The sample with the closest composition to ours ($x = 0.4$) was, however, only characterised at 1000 °C, yielding $D_O^* = 5.88 \times 10^{-7}$(cm^2/s). For $x = 0.25$, $D_O^* = 2.45 \exp(-(177 \pm 17\,\text{kJ mol}^{-1})/RT)$ (cm^2/s). These values agree reasonably well both in term of magnitude and activation energy with the values calculated for LSF-1250-15, which is the sample with the largest grains and thus the most susceptible to be representative of the grain properties. Nevertheless, it should be noted that our conductivity values are significantly smaller than those reported by other groups for the same or similar compositions.[12,18,19] Unfortunately, this discrepancy cannot be discussed further since no information about the microstructure of their samples is available.

3.3. TEM observations

Grain boundaries were examined in the LSF-1250-15 sample by transmission electron microscopy (TEM) taking care to keep a low illumination intensity to avoid irradiation damage or structural changes in boundaries. They exhibit typical contrasts of local strains attributed to interface dislocations at low magnification. Bright field imaging with higher magnification reveals that the thickness of the boundary is not uniform. Fig. 6 is a 550 nm over-focused image of an edge-on interface. Some discontinuities are visible in the intergrain Fresnel fringe (dark segments within the grain boundary, indicated by the arrows), which suggests that some extraneous material may be present locally. High-resolution imaging (0.17 nm at Scherzer defocus) confirms this view. No clear amorphous layer is obvious at the interface (Fig. 7). On some areas lattice planes from both grains join possibly by forming an interfacial edge dislocation (A), but on some other (B and C) their contrast vanishes close to the interface, indicating a possible layer or inclusions about 0.5 nm thick that is most probably amorphous. Energy-dispersive spectroscopy (EDS) analysis with an elliptical probe about 3 nm × 10 nm along the grain boundary, however, failed to reveal any significant change in composition compared to the grain.

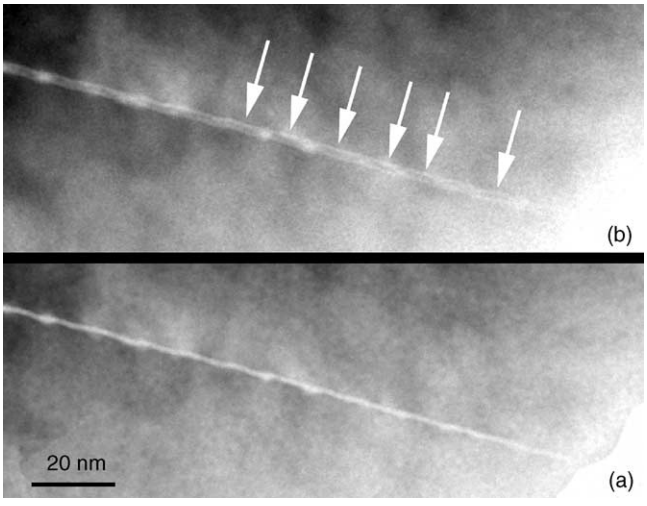

Fig. 6. Bright field images of a grain boundary at: (a) 550 nm underfocus and (b) 550 nm overfocus. The discontinuities observed along the dark intergrain Fresnel fringe suggest that some extraneous material may locally be present (arrows).

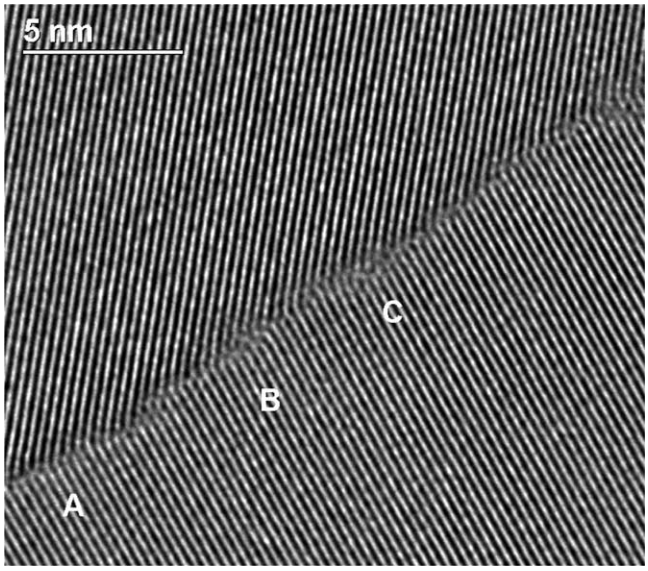

Fig. 7. High-resolution image of the interface between the two grains of Fig. 6 (near Scherzer defocus). The interface is wavy and interfacial edge dislocations are present where lattice planes join (A). On some areas the lattice plane contrast vanishes close to the interface (B and C) and some amorphous or foreign phase may be present in very thin layer (thickness less than 1 nm).

4. Conclusion

By measuring the oxygen permeation flux through $La_{0.5}Sr_{0.5}FeO_{3-\delta}$ membranes with different microstructures, the influence of the average size of the grains and/or the

length of the grain boundaries on the oxygen transport properties was examined. In particular, it was shown that the permeation flux was partially governed by surface limitation (fine grain, high temperature) and partially by bulk transport (coarse grain, low temperature). Only the bulk-limited fluxes were influenced by the grain size, with the higher values for the finer grains. This gives evidence of oxygen transport occurring preferentially along grain boundaries, which act as high diffusivity paths. Examination of the grain boundaries by transmission electron microscopy revealed typical contrasts of interface dislocations. The presence of extraneous material at the interface was suggested both by bright field and high resolution imaging, but no significant composition change could be found. Further investigations are still required for a clear explanation of the origin of the enhanced transport of oxygen along the grain boundaries.

Acknowledgements

This work was supported by the Swiss Federal Office for Science and Education (OFES) (COST action 525) and the Swiss National Science Foundation (Project 200021-100674/1). Fabienne Bobard is acknowledged for preparing the sample for TEM observation. Cristina Soare has kindly performed the TG-DTA measurements and Marlyse Demartin Maeder the dilatometer measurements.

References

1. Bouwmeester, H. J. M. and Burggraaf, A. J., Dense ceramic membranes for oxygen separation. In *The CRC Handbook of Solid State Electrochemistry*, ed. P. J. Gellings and H. J. M. Bouwmeester. CRC Press, Boca Raton, 1997, pp. 481–553.
2. Hammou, A. and Guindet, J., In *The CRC Handbook of Solid State Electrochemistry*, ed. P. J. Gellings and H. J. M. Bouwmeester. CRC Press, Boca Raton, 1997, p. 407.
3. Qiu, L., Lee, T. H., Liu, L.-M., Yang, Y. L. and Jacobson, A. J., Oxygen permeation studies of $SrCo_{0.8}Fe_{0.2}O_{3-\delta}$. *Solid State Ionics*, 1995, **76**, 321–329;
   Li, S., Jin, W., Huang, P., Xu, N., Shi, J., Lin, Y. S. *et al.*, Comparison of oxygen permeation and stability of perovskite type $La_{0.2}A_{0.8}Co_{0.2}Fe_{0.8}O_{3-\delta}$ (A = Sr, Ba, Ca) membranes. *Ind. Eng. Chem. Res.*, 1999, **38**, 2963–2972.
4. Zhang, K., Yang, Y., Jacobson, A. J. and Salama, K., *Mater. Res. Soc. Symp. Proc.*, 1998, **l496**, 341–346.
5. Zhang, K., Yang, Y., Ponnusamy, D., Jacobson, A. J. and Salama, K., Effect of microstructure on oxygen permeation in $SrCo_{0.8}Fe_{0.2}O_{3-\delta}$. *J. Mater. Sci.*, 1999, **34**, 1367–1372.
6. Kharton, V. V., Naumovich, E. N., Kovalevsky, A. V., Viskup, A. P., Figueredo, F. M., Bashmakov, I. A. *et al.*, Mixed electronic and ionic conductivity of $LaCo(M)O_3$ (M = Ga, Cr, Fe or Ni) IV. Effect of preparation methods on oxygen transport in $LaCoO_{3-\delta}$. *Solid State Ionics*, 2000, **138**, 135–148.
7. Qi, X., Lin, Y. S. and Swartz, S. L., Electric transport and oxygen permeation properties of lanthanum cobaltite membranes synthesized by different methods. *Ind. Eng. Chem. Res.*, 2000, **39**, 646–653.
8. Diethelm, S., Sfeir, J., Clemens, F., Van herle, J. and Favrat, D., Planar and tubular perovskite-type membrane reactors for partial oxidation of methane to syngas. *J. Solid State Electrochem.*, 2004, **8**, 611–617.
9. McAfee, R. and Nettleship, I., The simulation and selection of shapes for the unfolding of grain size distributions. *Acta Mater.*, 2003, **51**, 4603–4610.
10. Kingery, W. D., Bowen, H. K. and Uhlmann, D. R., *Introduction to Ceramics* (*2nd ed.*). John Wiley & Sons, New York, 1976, pp. 453–454.
11. Wagner, C., Equations for transport in solid oxides and sulfides of transition metals. *Prog. Solid State Chem.*, 1975, **10**, 3–16.
12. Patrakeev, M. V., Bahteeva, J. A., Mitberg, E. B., Leonidov, I. A., Kozhevnikov, V. L. and Poeppelmeier, K. R., Electron/hole and ion transport in $La_{1-x}Sr_xFeO_{3-\delta}$. *J. Solid State Chem.*, 2003, **172**, 219–231.
13. Incropera, F. P. and DeWitt, D. P., *Fundamentals of Heat and Mass Transfer* (*4th ed.*). John Wiley & Sons, New York, 1996, p. 590.
14. Kruidhof, H., Bouwmeester, H. J. M., van Doorn, R. H. E. and Burggraaf, A. J., Influence of order–disorder transitions on oxygen permeability through selected nonstoichiometric perovskite-type oxides. *Solid State Ionics*, 1993, **63–65**, 816–822.
15. Takeda, Y., Kanno, K., Takada, T., Yamamoto, O., Takano, M., Nakayama, N. *et al.*, Phase relation in the oxygen nonstoichiometric system $SrFeO_x$ ($2.5 \leq x \leq 3.0$). *J. Solid State Chem.*, 1986, **63**, 237–249.
16. Mizusaki, J., Yoshihiro, M., Yamauchi, S. and Fueki, K., Nonstoichiometry and defect structure of the perovskite-type oxides $La_{1-x}Sr_xFeO_{3-\delta}$. *J. Solid State Chem.*, 1985, **58**, 257–266.
17. Ishigaki, T., Yamauchi, S., Kishio, K., Mizusaki, J. and Fueki, K., Diffusion of oxide ion vacancies in perovskite-type oxides. *J. Solid State Chem.*, 1988, **73**, 179–187.
18. Teraoka, Y., Zhang, H. M., Okamoto, K. and Yamazoe, N., Mixed ionic-electronic conductivity of $La_{1-x}Sr_xCo_{1-y}Fe_yO_{3-\delta}$ perovskite-type oxides. *Mater. Res. Bull.*, 1988, **23**, 51–58.
19. Stevenson, J. W., Armstrong, T. R., Carneim, R. D., Pederson, L. R. and Weber, W. J., Electrochemical properties of mixed conducting perovskites $La_{1-x}M_xCo_{1-y}Fe_yO_{3-\delta}$ (M = Sr, Ba, Ca). *J. Electrochem. Soc.*, 1996, **143**, 2722–2729.